

EXPLORING SIMILARITY BETWEEN NEURAL AND LLM TRAJECTORIES IN LANGUAGE PROCESSING

Xin Xiao

School of Computer Science
Chongqing University
Chongqing, China
20241401023@stu.cqu.edu.cn

Kaiwen Wei*

School of Computer Science
Chongqing University
Chongqing, China
weikaiwen@cqu.edu.cn

Jiang Zhong*

School of Computer Science
Chongqing University
Chongqing, China
zhongjiang@cqu.edu.cn

Xuekai Wei

School of Computer Science
Chongqing University
Chongqing, China
xuekaiwei2-c@my.cityu.edu.hk

Mingliang Zhou

School of Computer Science
Chongqing University
Chongqing, China
mingliangzhou@cqu.edu.cn

ABSTRACT

Understanding the similarity between large language models (LLMs) and human brain activity is crucial for advancing both AI and cognitive neuroscience. In this study, we provide a multilinguistic, large-scale assessment of this similarity by systematically comparing 16 publicly available pretrained LLMs with human brain responses during natural language processing tasks in both English and Chinese. Specifically, we use ridge regression to assess the representational similarity between LLM embeddings and electroencephalography (EEG) signals, and analyze the similarity between the "neural trajectory" and the "LLM latent trajectory." This method captures key dynamic patterns, such as magnitude, angle, uncertainty, and confidence. Our findings highlight both similarities and crucial differences in processing strategies: (1) We show that middle-to-high layers of LLMs are central to semantic integration and correspond to the N400 component observed in EEG; (2) The brain exhibits continuous and iterative processing during reading, whereas LLMs often show discrete, stage-end bursts of activity, which suggests a stark contrast in their real-time semantic processing dynamics. This study could offer new insights into LLMs and neural processing, and also establish a critical framework for future investigations into the alignment between artificial intelligence and biological intelligence.

1 INTRODUCTION

The development of large language models (LLMs) has transformed natural language processing (NLP), enabling machines to generate human-like text and perform various linguistic tasks with impressive accuracy (Zhang et al., 2025; Lee et al., 2025; Zhang et al., 2024; Steyvers et al., 2025). However, the mechanisms by which LLMs process and understand language remain largely opaque (Takahashi et al., 2024; Ferraris et al., 2025; Rueda et al., 2025). This has spurred interest in comparing LLMs to human cognition, particularly regarding how both systems represent and process language. While LLMs excel at language tasks, the extent to which they simulate human cognitive processes is still an open research question.

*Corresponding author

Studies of AI-human similarity have traditionally focused on behavioral outcomes, comparing AI performance with human data across tasks such as essay writing, image recognition, and logical reasoning (Ashktorab et al., 2021; Kumar et al., 2024a; Mahner et al., 2025). While these comparisons suggest AI is becoming more human-like, they rely on behavioral data rather than neural evidence. Recently, research has shifted to exploring the alignment between AI mechanisms and human brain activity, particularly for LLMs. Neuroimaging techniques such as fMRI (Du et al., 2025), EEG (Xiao et al., 2025), MEG (Wehbe et al., 2014), and ECoG (Goldstein et al., 2022) have provided insights into the neural responses involved. Previous work has demonstrated alignment between LLMs and brain activity, primarily through linear mappings between neural responses and LLM representations (Zhou et al., 2024), such as activations, attention heads, and layer transformations (Caucheteux & King, 2022; Kumar et al., 2024b). These studies have examined various factors, including architectures and training conditions (Toneva & Wehbe, 2019; Mischler et al., 2024). LLM-brain alignment has also been used to investigate neural mechanisms, such as predictive processing and meaning composition, and to enhance both LLM performance and human-like language alignment (Rahimi et al., 2025; Moussa et al., 2024).

However, previous studies have largely focused on static correspondences or outcome-level similarities between LLM representations and neural responses, neglecting the temporal dynamics and processing trajectories that underpin human cognition. This raises an important question: *does this similarity stem solely from the convergent outputs of the models and the brain, or do these models emulate the underlying neural processing trajectory that govern human cognition?* This distinction is essential for understanding whether LLMs merely approximate brain activity or whether their internal computations reflect a deeper structural and functional resemblance to neural processes. As shown in Figure 1, our central motivation is to investigate this dynamic relationship by comparing the evolving EEG signals with the internal states of LLMs across layers, revealing the similarities and differences in their processing trajectories.

To investigate such similarities and differences between human cognitive processes and LLM computational trajectories, we conducted an experiment to compare EEG-extracted neural features with the text embeddings of 16 publicly available pretrained LLMs. Our analysis, based on English (Hollenstein et al., 2018) and Chinese (Mou et al., 2024) texts, focused on two key aspects: **representational similarity** and **trajectory similarity**. To evaluate representational similarity, we used ridge regression (McDonald, 2009) and applied metrics like Pearson correlation, Representational Similarity Analysis (RSA) (Freund et al., 2021), and Centered Kernel Alignment (CKA) (Saha et al., 2022) to quantify the correspondences between EEG signals and LLM representations. To analyze trajectory similarity across layers and time, we introduced Latent Trajectory Comparison (LTC) to analyze the similarity between "neural trajectory" of brain responses and the corresponding "LLM latent trajectory" from various aspects, including magnitude, angular changes, uncertainty, and confidence evolution. Our findings show that middle-to-high layers of LLMs play a key role in semantic integration, aligning with the N400 component in EEG, a marker of semantic processing. This suggests LLMs capture brain-like processing for semantic understanding. However, while the brain processes language continuously, LLMs exhibit discrete bursts of activity. Multi-linguistic comparisons reveal that LLMs align better with EEG for English, while the alignment is weaker for Chinese, suggesting that LLMs trained mainly on English data may struggle with the subtleties of non-English languages. **In conclusion, LLMs partially emulate neural processing trajectories by capturing temporal dynamics and semantic integration patterns observed in EEG, showing that this similarity goes beyond convergent outputs, albeit more discretely and segmentally than the brain.** Our main contributions could be summarized as follows:

1. We systematically compare LLMs and human brain activity, evaluating 16 publicly available pretrained LLMs in English and Chinese texts. Using ridge regression to model LLM

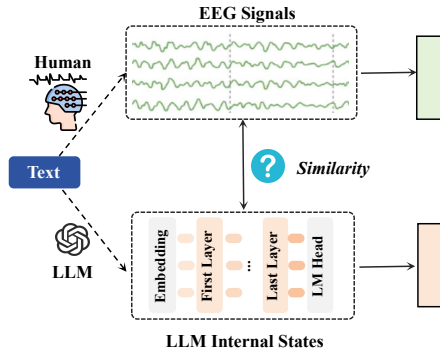


Figure 1: Comparison of human brain EEG signals and LLM internal states to explore similarities between human thought processes and model processing trajectories.

embeddings with EEG signals, we provide a large-scale, multilinguistic assessment of the similarity between LLM representations and neural activity in natural language processing.

2. Beyond static feature alignment, we analyse the temporal “neural trajectory” of brain responses and the corresponding “LLM latent trajectory” traced across hidden layers, incorporating measures of magnitude, angle, uncertainty, and confidence, providing insight into how dynamic neural processes relate to the evolving representations within LLMs.
3. Our analyses reveal that middle-to-high layers of LLMs generally serve as the core stage for hierarchical semantic integration. In contrast to the brain’s continuous and iterative recalibration during reading, LLMs often process information in delayed, stage-end bursts, highlighting distinct strategies in real-time semantic processing.

2 RELATED WORK

Neuroscientific Foundations of Language Comprehension. The neuroscience of language comprehension investigates the spatiotemporal dynamics of brain-based linguistic processing, spanning low-level perception to high-level semantic integration. Early work identified core “language network” regions, such as Broca’s area (syntax/production) (Flinker et al., 2015) and Wernicke’s area (semantics) (Ardila et al., 2016), but modern studies have refined this view to a distributed system. For example, fMRI research has shown that the left inferior frontal gyrus (LIFG), left middle temporal gyrus (LMTG), and angular gyrus (AG) collectively resolve syntactic ambiguities and integrate word meanings into coherent propositions (Noonan et al., 2013). With millisecond-level temporal resolution, EEG has further illuminated the timing of language processing via event-related potentials (ERPs) (Van Berkum et al., 2005). The N400 component (400 ms post-stimulus) responds to semantic anomalies, reflecting efforts to integrate unexpected words (Fogelson et al., 2004), and the P600 index syntactic reanalysis (Tanner et al., 2017). These ERPs act as neurophysiological markers for linguistic representation building, revealing intermediate processing steps overlooked by behavioral measures. Collectively, these findings establish that language comprehension is a dynamic, incremental process shaped by both bottom-up sensory input and top-down contextual expectations.

Brain Similarity of Language Models. Numerous studies have shown that deep neural network representations can be linearly mapped to neural responses (Toneva & Wehbe, 2019; Schrimpf et al., 2021; Anderson et al., 2021), suggesting that both human brains and language models are involved in predicting the next word (Schrimpf et al., 2021). Brain activation correlates with language models, peaking around 400 ms after word onset (Goldstein et al., 2022). Further work has explored aspects like autoregressive models (Goldstein et al., 2022; Caucheteux et al., 2023), model size, and linguistic generalizability (Caucheteux & King, 2022; Antonello & Huth, 2024), providing insights into the brain-like nature of language processing in LLMs. As models trained on massive text corpora, LLMs demonstrate emergent abilities in semantic parsing, context integration, and hierarchical processing (Li et al., 2024). Notably, embeddings from later LLM layers have been shown to correlate with fMRI and MEG responses during language comprehension, indicating partial alignment between computational and neural semantic representations (Zhou et al., 2024; Mischler et al., 2024; Nakagi et al., 2024; Rahimi et al., 2025; Lei et al., 2025; Du et al., 2025). For example, (Ren et al., 2024; Du et al., 2025) employed representational similarity analysis (RSA) to compare text embeddings with fMRI signals, constructing representational dissimilarity matrices (RDMs) via metrics such as Pearson correlation. Other studies (Zhou et al., 2024) aligned layerwise activations of language models with averaged MEG activity maps via ridge regression McDonald (2009). Additionally, (Tuckute et al., 2024) trained encoding models on fMRI data from participants exposed to diverse sentences, optimizing GPT-2 XL embeddings to enhance neural alignment. Unlike most existing studies that rely on static analysis, we differentiate our approach by quantifying dynamic alignment, offering a deeper understanding of the evolving EEG and LLM patterns and highlighting both shared and unique aspects of their interactions.

3 METHODOLOGY

To investigate the similarity between LLM representations and human neural activity during language comprehension, as summarized in Figure 2, we investigate two types of similarity: (1) for **representation similarity**, we predict EEG features from LLM embeddings using ridge regression,

and assess alignment through metrics such as Pearson correlation, RSA, spatiotemporal (ST) alignment, and functional connectivity. (2) for **trajectory similarity**, we apply latent trajectory comparison (LTC) to examine “neural trajectory” and “LLM latent trajectory” through various measures, including magnitude variations, angular shifts, uncertainty fluctuations, and confidence evolution.

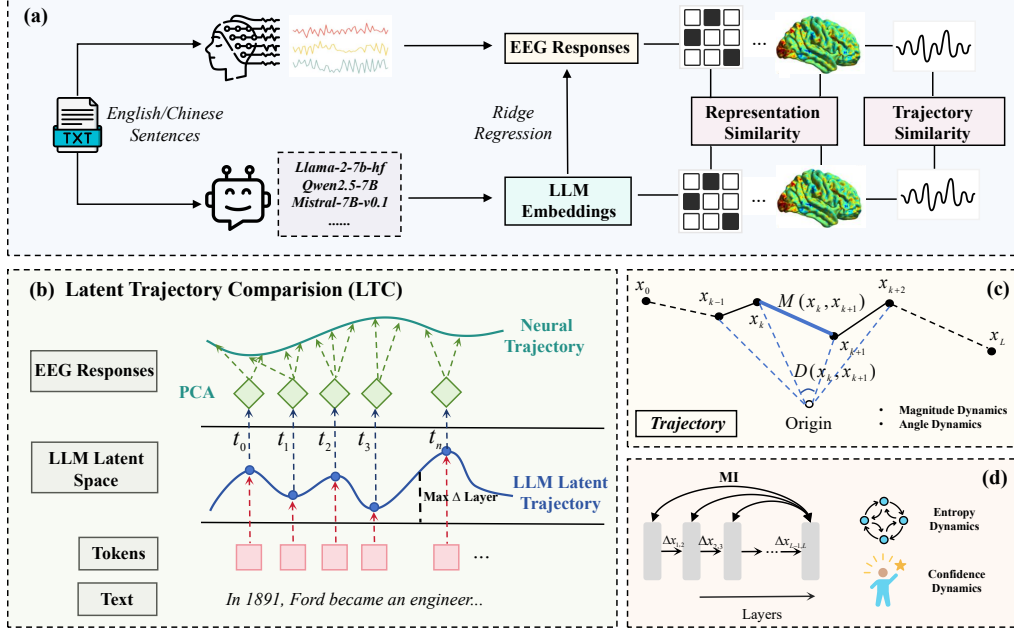


Figure 2: Overview of the proposed methodology for investigating brain-LLM language processing similarities. (a) Framework for measuring Representation similarity: Pearson correlation (ridge regression), spatiotemporal (ST) alignment, and latent trajectory comparison (LTC). (b) LTC: Trajectories across layers and time are compared. (c) Magnitude and angular dynamics: Analysing intensity and directionality. (d) Uncertainty and confidence dynamics.

3.1 REPRESENTATION SIMILARITY

To assess the alignment between LLM representations and human neural activity, we first assess representation similarity. Specifically, we process the text by segmenting it into sentences and feeding them into 16 pretrained LLMs. To quantify how semantic representations from different layers of LLMs relate to EEG activity, we employ ridge regression in a layerwise encoding framework. Let $M \in \mathbb{R}^{N \times d}$ denote the EEG responses and let $L \in \mathbb{R}^{N \times L \times D}$ denote the LLM embeddings, where N is the number of samples, L is the number of layers, and D is the embedding dimensionality. For each layer l and fold k in K -fold cross-validation, the ridge regression weights are estimated as:

$$\hat{W}^{(l,k)} = (L_{\text{train}}^{(l,k)\top} L_{\text{train}}^{(l,k)} + \alpha I)^{-1} L_{\text{train}}^{(l,k)\top} M_{\text{train}}^{(k)}, \quad (1)$$

where α is the regularization parameter selected via nested cross-validation. The predicted EEG responses for the test set are as follows:

$$\hat{M}_{i,\text{test}} = L_{i,\text{test}} \hat{W}^{(l,k)} + \hat{b}_i. \quad (2)$$

To quantify the representational similarity between predicted EEG \hat{M} and ground-truth EEG M , we employ RSA by computing RDMs (Du et al., 2025) for both and measuring similarity as the Spearman correlation between the upper triangular elements of RDM_M and $\text{RDM}_{\hat{M}}$, yielding an RSA score reflecting how well the predicted responses preserve the representational structure of true EEG. To capture global subspace alignment, we compute CKA (Cortes et al., 2012):

$$\text{CKA}(\hat{M}, M) = \frac{\|\hat{M}^\top M\|_F^2}{\|\hat{M}^\top \hat{M}\|_F \cdot \|M^\top M\|_F}, \quad (3)$$

where $\|\cdot\|_F$ is the Frobenius norm and where \hat{M} , M is mean-centered.

As a sanity check, we evaluate whether the predictive model could accurately capture both the spatial and temporal dynamics of language processing. We assess spatiotemporal alignment between EEG signals and LLM predictions by computing time-resolved, channelwise correlations to generate topographic maps. Functional connectivity (Fingelkurts et al., 2005) is quantified via Pearson correlations across channels within sliding time windows for both EEG and LLM-predicted responses. This captures the temporal evolution of neural activity and enables network-level comparisons.

3.2 LATENT TRAJECTORY COMPARISON

Building on representation similarity, we further explore trajectory similarity to capture the dynamic evolution of information processing in both brains and LLMs. Human cognition involves both fast, intuitive processes and slower, deliberative ones (Evans, 2003), similar to how LLMs process surface features in lower layers and semantics in higher layers (Wang et al., 2024). We compare the “neural trajectory” and “LLM latent trajectory,” tracking semantic evolution through measures like magnitude and angle changes, uncertainty, mutual information, skewness, kurtosis, Lyapunov exponent, and dynamic alignment, providing a holistic view of processing in both systems.

Trajectory Formalization. For both EEG and LLM, the “trajectory” is defined as a sequence of transformations across temporal steps or layers. The unified trajectory can be expressed as:

$$\mathbf{H} = \underbrace{\mathbf{h}_0}_{\text{initial state}} \rightarrow \underbrace{\mathbf{h}_1 \rightarrow \cdots \rightarrow \mathbf{h}_l \rightarrow \cdots \rightarrow \mathbf{h}_{L-1}}_{\text{intermediate states}} \rightarrow \underbrace{\mathbf{h}_L}_{\text{final state}}, \quad (4)$$

where for EEG, each \mathbf{h}_l represents the neural state at temporal window l , and for LLM, each \mathbf{h}_l denotes the hidden state at layer l .

Magnitude and Angle Dynamics. We compare the geometric features of the EEG and LLM trajectory by examining the magnitude and angle changes between adjacent states in the embedding trajectory. Both the magnitude change $M(\mathbf{h}_l, \mathbf{h}_{l+1})$ and the angle change $A(\mathbf{h}_l, \mathbf{h}_{l+1})$ are:

$$M(\mathbf{h}_l, \mathbf{h}_{l+1}) = \|\mathbf{h}_{l+1} - \mathbf{h}_l\|_2, \quad A(\mathbf{h}_l, \mathbf{h}_{l+1}) = \arccos\left(\frac{\mathbf{h}_{l+1}^\top \mathbf{h}_l}{\|\mathbf{h}_{l+1}\|_2 \|\mathbf{h}_l\|_2}\right). \quad (5)$$

where $M(\mathbf{h}_l, \mathbf{h}_{l+1})$ quantifies the distance between consecutive states, and $A(\mathbf{h}_l, \mathbf{h}_{l+1})$ measures the angular change, which indicates the directional shift in the trajectory.

To normalize the absolute changes across different trajectories, we define the average magnitude and angle over the entire trajectory as follows:

$$\text{Mag}(\mathbf{H}) = \frac{1}{L} \sum_{l=0}^{L-1} \frac{M(\mathbf{h}_l, \mathbf{h}_{l+1})}{\mathcal{Z}_{\text{Mag}}}, \quad \text{Ang}(\mathbf{H}) = \frac{1}{L} \sum_{l=0}^{L-1} \frac{A(\mathbf{h}_l, \mathbf{h}_{l+1})}{\mathcal{Z}_{\text{Ang}}}, \quad (6)$$

where \mathcal{Z}_{Mag} and \mathcal{Z}_{Ang} are scaling factors used to normalize the absolute magnitude and angle changes relative to the overall trajectory.

Uncertainty and Confidence Dynamics. The dynamics of uncertainty and confidence reveal how a system accumulates and processes information over time. We focus on matrix-based entropy (Yu et al., 2021; Skean et al., 2025), a comprehensive metric that quantifies uncertainty while considering both compression and variability in the system’s representations (see Appendix A.1 for details). Let $Z \in \mathbb{R}^{N \times D}$ be the matrix of hidden states at time step k . We define the Gram matrix $K = ZZ^\top$, which captures pairwise relationships between data points. The matrix-based entropy $S_\alpha(Z)$ for order $\alpha > 0$ is as follows:

$$S_\alpha(Z) = \frac{1}{1-\alpha} \log\left(\sum_{i=1}^r \left(\frac{\lambda_i(K)}{\text{tr}(K)}\right)^\alpha\right) \quad (7)$$

where $r = \text{rank}(K) \leq \min(N, D)$, $\lambda_i(K)$ are the eigenvalues of K , and $\text{tr}(K)$ is the trace. We typically use $\alpha = 1$ for simplicity, as it simplifies the entropy measure to von Neumann entropy.

Confidence can be interpreted as the inverse of uncertainty, providing a complementary view of system dynamics. For each stage:

$$C^{(X)}(k) = \frac{1}{S_\alpha(Z) + \epsilon} \bigg/ \max_{k'} \frac{1}{S_\alpha(Z) + \epsilon} \quad (8)$$

This normalizes confidence to a 0–1 scale, with $\epsilon = 10^{-8}$, ensuring numerical stability.

Mutual Information. Mutual information (MI) (Kraskov et al., 2004) measures the shared information between two variables, reflecting their dependence. In both EEG signals and LLMs, MI captures the relationship between intermediate layers and the final output, revealing how information propagates. For both EEG signals and LLMs, the mutual information between an intermediate layer \mathbf{h}_i and the final output \mathbf{h}_L is given by:

$$I(\mathbf{h}_i, \mathbf{h}_L) = \sum_{x \in \mathbf{h}_i} \sum_{y \in \mathbf{h}_L} p(x, y) \log \left(\frac{p(x, y)}{p(x)p(y)} \right) \quad (9)$$

where \mathbf{h}_i refers to the intermediate layer embedding and \mathbf{h}_L represents the final output layer.

Skewness, Kurtosis, and Lyapunov Exponent. Skewness and kurtosis (Groeneveld & Meeden, 1984) quantify EEG and LLM feature asymmetry and peakness, while the Lyapunov exponent (Young, 2013) measures sensitivity to initial conditions, with positive values indicating chaos.

Dynamic Representational Alignment (DRA). We propose a metric DRA (Appendix A.3) on the Hilbert space \mathbf{H} (Young, 1988), where EEG representations $\mathbf{E}(t) \in \mathbf{H}_{\text{EEG}}^d$ and LLM hidden states $\mathbf{L}(t) \in \mathbf{H}_{\text{LLM}}^k$ have bounded norms. DRA incorporates Gaussian distribution divergence to penalize shifts and applies a probabilistic weight to emphasize important time steps. The formulation is:

$$\text{DRA} = \frac{1}{Z_T} \sum_{t=1}^T \omega(t) \cdot \cos(\mathbf{E}(t), \mathbf{L}(t)) \cdot \frac{\langle \Delta \mathbf{E}(t), \Delta \mathbf{L}(t) \rangle_{\mathbf{H}}}{|\Delta \mathbf{E}(t)|_{\mathbf{H}} |\Delta \mathbf{L}(t)|_{\mathbf{H}} + \epsilon} \cdot e^{-\alpha \cdot \text{KL}(P_t \| Q_t)} \quad (10)$$

where Z_T is an ℓ_2 -normalization factor to keep DRA in $[0, 1]$; $\omega(t) \propto \text{Gamma}(t; \beta, 1)$ ($\beta > 0$) weights time-step importance; $P_t = \mathcal{N}(\mu_{\mathbf{E}(t)}, \Sigma_{\mathbf{E}(t)})$ and $Q_t = \mathcal{N}(\mu_{\mathbf{L}(t)}, \Sigma_{\mathbf{L}(t)})$ are EEG or LLM Gaussian representations with $\text{KL}(\cdot \| \cdot)$ the Kullback-Leibler divergence; $\epsilon = 10^{-8}$ ensures numerical stability; $\alpha \in (0, 5]$ controls the divergence penalty.

4 EXPERIMENTS AND RESULTS

4.1 DATA PREPARATION AND PREPROCESSING

Many studies linking brain activity and LLMs have used fMRI (Du et al., 2025; Lei et al., 2025), but its low temporal resolution limits tracking word-level processing. To overcome this, we use EEG for the first time, which capture millisecond-level neural dynamics during language comprehension, across two datasets: (1) **ZuCo Dataset** (Hollenstein et al., 2018): English EEGs and eye-tracking data from 12 participants reading 1,050 sentences (movie reviews and Wikipedia) under normal reading (NR). The data were recorded with a 128-channel Geodesic Hydrocel system at 500 Hz and preprocessed with artifact rejection, interpolation, and rereferencing. (2) **ChineseEEG Dataset** (Mou et al., 2024): Chinese text reading EEGs from 10 participants (The Little Prince and Garnett Dream, 115,233 characters) using a 128-channel system at 1 kHz, preprocessed with segmentation, downsampling, filtering, ICA denoising, and referencing.

To provide a comprehensive evaluation across diverse architectures, we employ a set of sixteen state-of-the-art, publicly available LLMs from the HuggingFace¹ repositories. These models span multiple families (LLaMA (Touvron et al., 2023), Qwen (Hui et al., 2024), Mistral (Siino, 2024), Gemma (Team et al., 2024), Falcon (Almazrouei et al., 2023), Yi (Young et al., 2024), DeepSeek (Bi et al., 2024)) and cover both *base* and *instruction-tuned* variants (see Appendix A.4).

4.2 MODEL CORRELATION PERFORMANCE

Table 1 summarizes the similarity results for 16 LLMs, evaluated using mean squared error (MSE), Pearson correlation (r), representational similarity analysis (RSA), and centered kernel alignment (CKA). On the ZuCo dataset, gemma-7b-it achieved the highest Pearson correlation of 0.5103, while Meta-Llama-3-8B-Instruct attained the best CKA score of 0.4350. Instruction-tuned variants consistently outperformed their base models, indicating that instruction tuning improves representational

¹<https://huggingface.co/>

Table 1: Sentence-level alignment results between LLM representations and brain signals for both English and Chinese datasets. Best results per column are in **bold**.

Model	ZuCo Dataset				ChineseEEG Dataset			
	MSE ↓	r ↑	RSA ↑	CKA ↑	MSE ↓	r ↑	RSA ↑	CKA ↑
Llama-2-7b-hf	0.8370	0.4809	0.3987	0.3967	1.1821	0.1675	0.1354	0.3936
Llama-2-7b-chat-hf	0.8340	0.4951	0.4360	0.3931	1.2163	0.1320	0.1298	0.3762
Meta-Llama-3-8B	0.8257	0.4980	0.4044	0.4125	1.2157	0.1475	0.1381	0.3697
Meta-Llama-3-8B-Instruct	0.8128	0.5026	0.4220	0.4350	1.2194	0.1349	0.1293	0.3429
Qwen2.5-7B	0.9834	0.3828	0.2064	0.2841	1.2639	0.0702	0.1086	0.2794
Qwen2.5-7B-Instruct	0.9806	0.3832	0.2068	0.2778	1.2564	0.0789	0.1120	0.2946
Mistral-7B-v0.1	0.8117	0.4681	0.3477	0.4169	1.2218	0.1210	0.1172	0.3737
Mistral-7B-Instruct-v0.1	0.8268	0.4714	0.3852	0.4127	1.2171	0.1338	0.1410	0.3887
gemma-7b	0.8678	0.4841	0.4160	0.3990	1.2331	0.1552	0.1379	0.3127
gemma-7b-it	0.8140	0.5103	0.3824	0.3852	1.2444	0.1308	0.1084	0.2815
Falcon3-7B-Base	0.8855	0.4416	0.3481	0.3689	1.2130	0.1098	0.1116	0.3553
Falcon3-7B-Instruct	0.8842	0.4396	0.3368	0.3685	1.2298	0.1493	0.1352	0.3435
Yi-1.5-9B	0.8679	0.4302	0.2909	0.3481	1.2072	0.1218	0.1105	0.3754
Yi-1.5-9B-Chat	0.8937	0.4508	0.3097	0.2969	1.2663	0.0489	0.0697	0.2536
deepseek-llm-7b-base	0.8261	0.4886	0.3822	0.4021	1.2510	0.0751	0.0888	0.2436
DeepSeek-R1-Distill-Qwen-7B	0.9919	0.3554	0.2593	0.3104	1.2375	0.1029	0.0690	0.2386

alignment with neural responses. In contrast, Pearson correlation on the ChineseEEG dataset was generally lower. Yi-1.5-9B had the lowest MSE of 1.2072, while Llama-2-7b-hf scored highest in correlation and CKA. Mistral-7B-Instruct-v0.1 achieved the best RSA score. Unlike the English dataset, base models often outperformed instruction-tuned variants on Chinese, likely due to limited high-quality Chinese instruction data and the predominance of English optimization in instruction tuning, leading to mismatches with Chinese linguistic and cultural nuances.

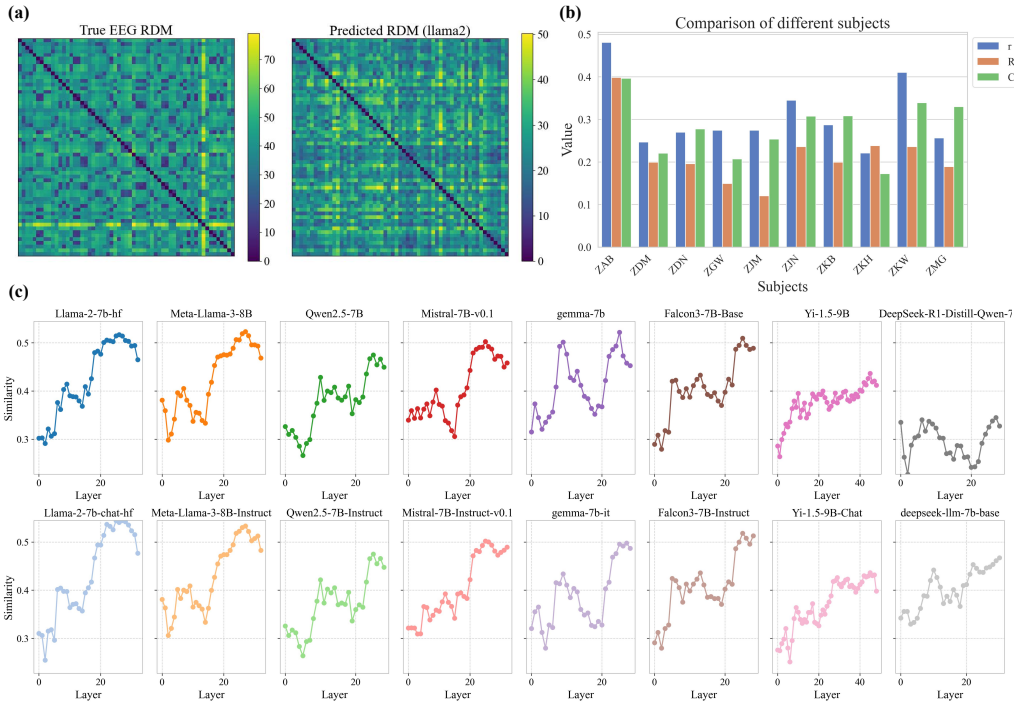


Figure 3: Similarity analysis. (a) Visualization of EEG-LLM similarity via RDMs. (b) Comparison across different subjects. (c) Trend of similarity between LLM layers and EEG responses.

As shown in Figure 3 (a), representational dissimilarity matrices computed from EEG and ridge-regressed LLM predictions via Euclidean distances exhibit similar spatial patterns. The correlation of the upper-triangular elements revealed a significant positive relationship ($R = 0.4066, p < 0.05$), indicating that LLMs partially capture human representational structures. Figure 3 (b) presents the results of similarity analysis for different subjects. subject ZAB has the highest values for all the metrics, whereas ZIM has a relatively low RSA. Generally, Pearson correlation tends to be greater than RSA and CKA, suggesting that the Pearson correlation captures stronger neural-model associations in this study. Figure 3 (c) presents the similarity curves between different layers of the LLMs and EEG signals, the layer similarity curves of all the models exhibit nonmonotonic fluctuations, with peaks typically occurring in the middle-to-high layers (10–30). These findings suggest that these layers play a key role in integrating in-depth features during the hierarchical semantic processing of LLMs.

4.3 SPATIOTEMPORAL PATTERNS OF PREDICTIONS

The EEG-LLM correlation topomaps in Figure 4 (a) reveal dynamic spatial patterns of similarity across time. In the early stage (0–200 ms), EEG shows positive correlations for sensory processing, with negative correlations around 100 ms indicating categorization and filtering. In the mid-stage (200–400 ms), significant positive correlations appear, particularly around 300 ms, corresponding to semantic integration and syntactic analysis. It suggests that LLMs simulate the brain’s semantic network and syntactic processing. In the later stage (400–500 ms), central–anterior effects at 400 ms align with the N400 component, reflecting semantic integration during language comprehension. EEG topographies show involvement of key language areas, such as Broca’s and Wernicke’s areas, aligning with LLM’s attention mechanisms. Hemispheric asymmetry, especially right-side correlations at 300 ms, mirrors the lateralization of language processing, indicating a correspondence between LLMs and brain hemispheric specialization (Van Berkum et al., 2005; Tanner et al., 2017).

EEG functional connectivity shows sparse but strong links among core regions with weak global coupling, reflecting “functional differentiation with efficient coordination.” In contrast, LLM-predicted connectivity is densely distributed, suggesting “global generalization with diminished regional specificity” and limited fidelity to biological networks. Both modalities highlight strong central and temporal language-related connectivity, indicating that LLMs capture the core collaborative network for language. However, weak frontal–occipital links in EEG (Figure 4 (b)) are overestimated in LLMs (Figure 4 (c)), and temporal–limbic connections are underrepresented, underscoring insufficient modelling of cross-functional coordination and limbic contributions.

4.4 LATENT TRAJECTORY COMPARISON

Magnitude and Angle Patterns. As shown in Figure 5 (a) and (b), the features reveal distinct temporal dynamics between EEGs and LLMs. In terms of magnitude, EEGs exhibit continuous fluctuations with early peaks at steps 5 and 17, reflecting rapid, distributed, and iterative neural processing, whereas LLMs remain largely stable before a sharp surge at step 31, resembling a “silent analysis followed by late integration.” Angle patterns show a similar divergence: EEGs display irregular peaks at steps 5, 12, and 25, which is consistent with ongoing neural reorientation, whereas LLMs rise gradually and spike only at step 31, suggesting sequential and hierarchical adjustment. Together, these results highlight a contrast between the brain’s real-time semantic recalibration and the model’s delayed, stage–end consolidation (see Appendix A.5 for Chinese EEG datasets).

Uncertainty and Confidence Dynamics. As shown in Figure 5 (c) and (d), LLMs start with high entropy, which rapidly decreases, whereas confidence gradually increases and peaks around Layer 30, reflecting a delayed, stage-like consolidation of uncertainty resolution. In contrast, EEGs maintain relatively stable entropy fluctuations alongside frequent confidence peaks and troughs, which is consistent with continuous real-time adjustment. The vertical dashed lines highlight critical transition points, underscoring the divergence between the brain’s dynamic recalibration and the model’s late integration strategy.

MI Dynamics. The MI dynamics shown in Figure 5 (e) reveal a clear divergence in information coupling: EEG show sharp, high-amplitude peaks, whereas LLM data display a gradual, low-amplitude rise, indicating distinct temporal modes of information integration during language processing.

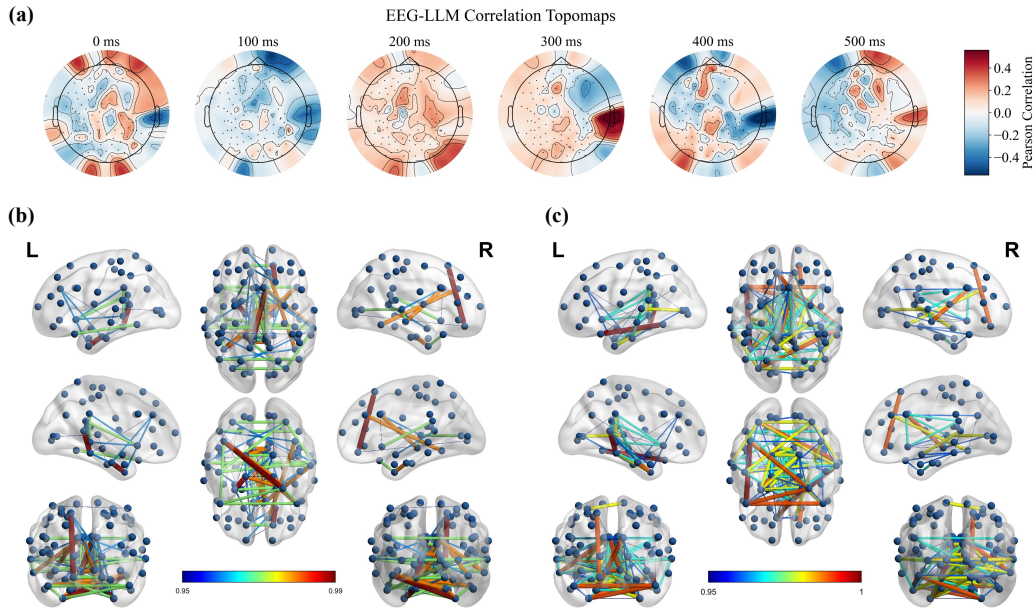


Figure 4: Topographic maps and connectivity analysis. (a) Topographic maps of EEG–LLM correlations. (b) EEG functional connectivity patterns. (c) Functional connectivity predicted by LLM.

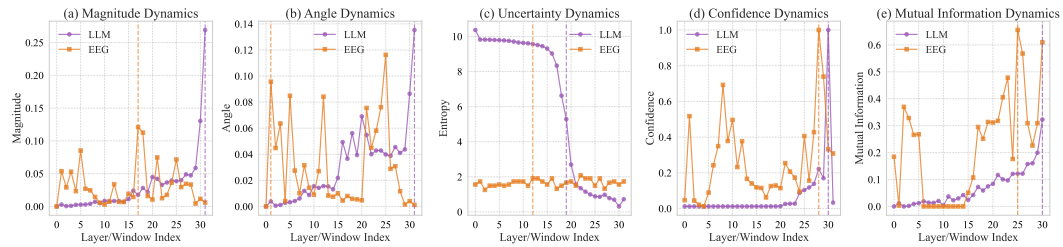


Figure 5: Temporal and dynamic comparisons between EEGs and LLMs. (a) Magnitude dynamics, (b) Angle dynamics, (c) Uncertainty dynamics, (d) Confidence dynamics, (e) MI dynamics.

Alignment. This section compares the alignment between the “neural trajectory” and “LLM latent trajectory” for English and Chinese, using metrics like entropy, magnitude, skewness, kurtosis, and others to assess EEG–LLM correspondence. As shown in Figure 6, the alignment shows clear language-dependent differences. Entropy alignment is higher in Chinese, indicating stronger structural similarity. MI alignment is higher in English, reflecting tighter information coupling. Magnitude and angular alignment are elevated in Chinese, suggesting stronger directional and amplitude consistency. Lyapunov exponents indicate slightly greater EEG instability in Chinese data, while LLM trajectories remain stable. Distributional properties further differ: Chinese EEG signals are negatively skewed with higher kurtosis, whereas LLM features show positive skew and lighter tails.

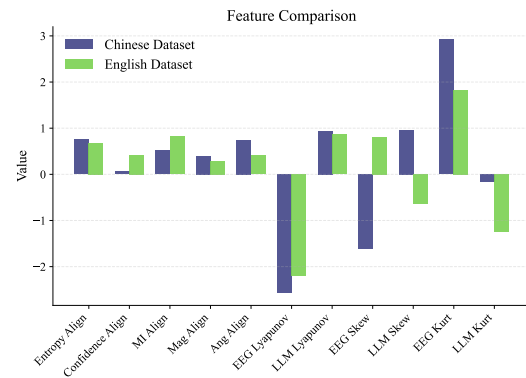


Figure 6: Alignment comparison across features between the English and Chinese datasets.

5 CONCLUSION

In this work, we present a multilingual assessment of the similarity between human brain activity and LLMs. By comparing 16 publicly available pretrained LLMs with human EEG responses during natural language processing tasks in both English and Chinese, we evaluated their similarity from the perspectives of representational similarity and trajectory similarity. We used ridge regression to quantify the alignment between LLM embeddings and EEG signals, and further analyzed the trajectory evolution of information processing. Our findings show that middle-to-high layers of LLMs are crucial for semantic integration, and while the brain continuously adjusts during reading, LLMs often process information in discrete, stage-end bursts. This study offers valuable insights into both the shared and distinct computational strategies of the brain and LLMs, contributing to the development of more human-like models.

REFERENCES

- Ebtesam Almazrouei, Hamza Alobeidli, Abdulaziz Alshamsi, Alessandro Cappelli, Ruxandra Cojocaru, M erouane Debbah,  tienne Goffinet, Daniel Hesslow, Julien Launay, Quentin Malartic, et al. The falcon series of open language models. *arXiv preprint arXiv:2311.16867*, 2023.
- Andrew James Anderson, Douwe Kiela, Jeffrey R Binder, Leonardo Fernandino, Colin J Humphries, Lisa L Conant, Rajeev DS Raizada, Scott Grimm, and Edmund C Lalor. Deep artificial neural networks reveal a distributed cortical network encoding propositional sentence-level meaning. *Journal of Neuroscience*, 41(18):4100–4119, 2021.
- Richard Antonello and Alexander Huth. Predictive coding or just feature discovery? an alternative account of why language models fit brain data. *Neurobiology of Language*, 5(1):64–79, 2024.
- Alfredo Ardila, Byron Bernal, and Monica Rosselli. The role of wernicke’s area in language comprehension. *Psychology & Neuroscience*, 9(3):340, 2016.
- Zahra Ashktorab, Casey Dugan, James Johnson, Qian Pan, Wei Zhang, Sadhana Kumaravel, and Murray Campbell. Effects of communication directionality and ai agent differences in human-ai interaction. In *Proceedings of the 2021 CHI conference on human factors in computing systems*, pp. 1–15, 2021.
- Xiao Bi, Deli Chen, Guanting Chen, Shanhuang Chen, Damai Dai, Chengqi Deng, Honghui Ding, Kai Dong, Qiushi Du, Zhe Fu, et al. Deepseek llm: Scaling open-source language models with longtermism. *arXiv preprint arXiv:2401.02954*, 2024.
- Laurent Bonnasse-Gahot and Christophe Pallier. fmri predictors based on language models of increasing complexity recover brain left lateralization. *Advances in Neural Information Processing Systems*, 37:125231–125263, 2024.
- Charlotte Caucheteux and Jean-R emi King. Brains and algorithms partially converge in natural language processing. *Communications biology*, 5(1):134, 2022.
- Charlotte Caucheteux, Alexandre Gramfort, and Jean-R emi King. Evidence of a predictive coding hierarchy in the human brain listening to speech. *Nature human behaviour*, 7(3):430–441, 2023.
- Songlin Chen, Weicheng Wang, Xiaoliang Chen, Maolin Zhang, Peng Lu, Xianyong Li, and Yajun Du. Enhancing chinese comprehension and reasoning for large language models: an efficient lora fine-tuning and tree of thoughts framework. *The Journal of Supercomputing*, 81(1):50, 2025.
- Corinna Cortes, Mehryar Mohri, and Afshin Rostamizadeh. Algorithms for learning kernels based on centered alignment. *The Journal of Machine Learning Research*, 13(1):795–828, 2012.
- Changde Du, Kaicheng Fu, Bincheng Wen, Yi Sun, Jie Peng, Wei Wei, Ying Gao, Shengpei Wang, Chuncheng Zhang, Jinpeng Li, et al. Human-like object concept representations emerge naturally in multimodal large language models. *Nature Machine Intelligence*, pp. 1–16, 2025.
- Jonathan St BT Evans. In two minds: dual-process accounts of reasoning. *Trends in cognitive sciences*, 7(10):454–459, 2003.

- Andrea Filippo Ferraris, Davide Audrito, Luigi Di Caro, and Cristina Poncibò. The architecture of language: Understanding the mechanics behind llms. In *Cambridge Forum on AI: Law and Governance*, volume 1, pp. e11. Cambridge University Press, 2025.
- Andrew A Fingelkurts, Alexander A Fingelkurts, and Seppo Kähkönen. Functional connectivity in the brain—is it an elusive concept? *Neuroscience & Biobehavioral Reviews*, 28(8):827–836, 2005.
- Adeen Flinker, Anna Korzeniewska, Avgusta Y Shestyuk, Piotr J Franaszczuk, Nina F Dronkers, Robert T Knight, and Nathan E Crone. Redefining the role of broca’s area in speech. *Proceedings of the National Academy of Sciences*, 112(9):2871–2875, 2015.
- Noa Fogelson, Constantinos Loukas, John Brown, and Peter Brown. A common n400 eeg component reflecting contextual integration irrespective of symbolic form. *Clinical Neurophysiology*, 115(6):1349–1358, 2004.
- Michael C Freund, Joset A Etzel, and Todd S Braver. Neural coding of cognitive control: the representational similarity analysis approach. *Trends in Cognitive Sciences*, 25(7):622–638, 2021.
- Ariel Goldstein, Zaid Zada, Eliav Buchnik, Mariano Schain, Amy Price, Bobbi Aubrey, Samuel A Nastase, Amir Feder, Dotan Emanuel, Alon Cohen, et al. Shared computational principles for language processing in humans and deep language models. *Nature neuroscience*, 25(3):369–380, 2022.
- Richard A Groeneveld and Glen Meeden. Measuring skewness and kurtosis. *Journal of the Royal Statistical Society Series D: The Statistician*, 33(4):391–399, 1984.
- Nora Hollenstein, Jonathan Rotsztejn, Marius Troendle, Andreas Pedroni, Ce Zhang, and Nicolas Langer. Zuco, a simultaneous eeg and eye-tracking resource for natural sentence reading. *Scientific data*, 5(1):1–13, 2018.
- Eghbal Hosseini and Evelina Fedorenko. Large language models implicitly learn to straighten neural sentence trajectories to construct a predictive representation of natural language. *Advances in Neural Information Processing Systems*, 36:43918–43930, 2023.
- Binyuan Hui, Jian Yang, Zeyu Cui, Jiayi Yang, Dayiheng Liu, Lei Zhang, Tianyu Liu, Jiajun Zhang, Bowen Yu, Keming Lu, et al. Qwen2. 5-coder technical report. *arXiv preprint arXiv:2409.12186*, 2024.
- Alexander Kraskov, Harald Stögbauer, and Peter Grassberger. Estimating mutual information. *Physical Review E—Statistical, Nonlinear, and Soft Matter Physics*, 69(6):066138, 2004.
- Nathan Krislock and Henry Wolkowicz. Euclidean distance matrices and applications. In *Handbook on semidefinite, conic and polynomial optimization*, pp. 879–914. Springer, 2012.
- Shashank Kumar, Sneha Tiwari, Rishabh Prasad, Abhay Rana, and MK Arti. Comparative analysis of human and ai generated text. In *2024 11th international conference on signal processing and integrated networks (SPIN)*, pp. 168–173. IEEE, 2024a.
- Sreejan Kumar, Theodore R Sumers, Takateru Yamakoshi, Ariel Goldstein, Uri Hasson, Kenneth A Norman, Thomas L Griffiths, Robert D Hawkins, and Samuel A Nastase. Shared functional specialization in transformer-based language models and the human brain. *Nature communications*, 15(1):5523, 2024b.
- Jung Hyun Lee, June Yong Yang, Byeongho Heo, Dongyoon Han, Kyungsu Kim, Eunho Yang, and Kang Min Yoo. Token-supervised value models for enhancing mathematical problem-solving capabilities of large language models. In *13th International Conference on Learning Representations, ICLR 2025*, pp. 11141–11160. International Conference on Learning Representations, ICLR, 2025.
- Yu Lei, Xingyang Ge, Yi Zhang, Yiming Yang, and Bolei Ma. Do large language models think like the brain? sentence-level evidence from fmri and hierarchical embeddings. *arXiv preprint arXiv:2505.22563*, 2025.

- Chuyuan Li, Yuwei Yin, and Giuseppe Carenini. Dialogue discourse parsing as generation: a sequence-to-sequence llm-based approach. In *Proceedings of the 25th annual meeting of the special interest group on discourse and dialogue*, pp. 1–14, 2024.
- Florian P Mahner, Lukas Muttenthaler, Umut Güçlü, and Martin N Hebart. Dimensions underlying the representational alignment of deep neural networks with humans. *Nature Machine Intelligence*, 7(6):848–859, 2025.
- Gary C McDonald. Ridge regression. *Wiley Interdisciplinary Reviews: Computational Statistics*, 1(1):93–100, 2009.
- Gavin Mischler, Yinghao Aaron Li, Stephan Bickel, Ashesh D Mehta, and Nima Mesgarani. Contextual feature extraction hierarchies converge in large language models and the brain. *Nature Machine Intelligence*, 6(12):1467–1477, 2024.
- Amai Momo, Kazomi Tanakashi, Gokuro Masanaka, Kyuji Mazano, and Benko Tanaka. Dynamic semantic contextualization in large language models via recursive context layering. *Authorea Preprints*, 2024.
- Xinyu Mou, Cuilin He, Liwei Tan, Junjie Yu, Huadong Liang, Jianyu Zhang, Yan Tian, Yu-Fang Yang, Ting Xu, Qing Wang, et al. Chineseeeg: A chinese linguistic corpora eeg dataset for semantic alignment and neural decoding. *Scientific Data*, 11(1):550, 2024.
- Omer Moussa, Dietrich Klakow, and Mariya Toneva. Improving semantic understanding in speech language models via brain-tuning. *arXiv preprint arXiv:2410.09230*, 2024.
- Yuko Nakagi, Takuya Matsuyama, Naoko Koide-Majima, Hiroto Q Yamaguchi, Rieko Kubo, Shinji Nishimoto, and Yu Takagi. Unveiling multi-level and multi-modal semantic representations in the human brain using large language models. *bioRxiv*, pp. 2024–02, 2024.
- Krist A Noonan, Elizabeth Jefferies, Maya Visser, and Matthew A Lambon Ralph. Going beyond inferior prefrontal involvement in semantic control: evidence for the additional contribution of dorsal angular gyrus and posterior middle temporal cortex. *Journal of cognitive neuroscience*, 25(11):1824–1850, 2013.
- Subba Reddy Oota, Akshett Jindal, Ishani Mondal, Khushbu Pahwa, Satya Sai Srinath Namburi, Manish Shrivastava, Maneesh Singh, Bapi S Raju, and Manish Gupta. Correlating instruction-tuning (in multimodal models) with vision-language processing (in the brain). *arXiv preprint arXiv:2505.20029*, 2025.
- N Pradhan and D Narayana Dutt. A nonlinear perspective in understanding the neurodynamics of eeg. *Computers in biology and medicine*, 23(6):425–442, 1993.
- Maryam Rahimi, Yadollah Yaghoobzadeh, and Mohammad Reza Daliri. Explanations of deep language models explain language representations in the brain. *arXiv e-prints*, pp. arXiv–2502, 2025.
- Yuqi Ren, Renren Jin, Tongxuan Zhang, and Deyi Xiong. Do large language models mirror cognitive language processing? *arXiv preprint arXiv:2402.18023*, 2024.
- Alice Rueda, Mohammed S Hassan, Argyrios Perivolaris, Bazen G Teferra, Reza Samavi, Sirisha Rambhatla, Yuqi Wu, Yanbo Zhang, Bo Cao, Divya Sharma, et al. Understanding llm scientific reasoning through promptings and model’s explanation on the answers. *arXiv preprint arXiv:2505.01482*, 2025.
- Aninda Saha, Alina Bialkowski, and Sara Khalifa. Distilling representational similarity using centered kernel alignment (cka). In *Proceedings of the the 33rd British Machine Vision Conference (BMVC 2022)*. British Machine Vision Association, 2022.
- Martin Schrimpf, Idan Asher Blank, Greta Tuckute, Carina Kauf, Eghbal A Hosseini, Nancy Kanwisher, Joshua B Tenenbaum, and Evelina Fedorenko. The neural architecture of language: Integrative modeling converges on predictive processing. *Proceedings of the National Academy of Sciences*, 118(45):e2105646118, 2021.

- Marco Siino. Mistral at semeval-2024 task 5: Mistral 7b for argument reasoning in civil procedure. In *Proceedings of the 18th International Workshop on Semantic Evaluation (SemEval-2024)*, pp. 155–162, 2024.
- Oscar Skean, Md Rifat Arefin, Dan Zhao, Niket Patel, Jalal Naghiyev, Yann LeCun, and Ravid Shwartz-Ziv. Layer by layer: Uncovering hidden representations in language models. *arXiv preprint arXiv:2502.02013*, 2025.
- Mark Steyvers, Heliodoro Tejeda, Aakriti Kumar, Catarina Belem, Sheer Karny, Xinyue Hu, Lukas W Mayer, and Padhraic Smyth. What large language models know and what people think they know. *Nature Machine Intelligence*, 7(2):221–231, 2025.
- Soh Takahashi, Masaru Sasaki, Ken Takeda, and Masafumi Oizumi. Self-supervised learning facilitates neural representation structures that can be unsupervisedly aligned to human behaviors. In *ICLR 2024 Workshop on Representational Alignment*, 2024.
- Darren Tanner, Sarah Grey, and Janet G van Hell. Dissociating retrieval interference and reanalysis in the p600 during sentence comprehension. *Psychophysiology*, 54(2):248–259, 2017.
- Gemma Team, Thomas Mesnard, Cassidy Hardin, Robert Dadashi, Surya Bhupatiraju, Shreya Pathak, Laurent Sifre, Morgane Rivière, Mihir Sanjay Kale, Juliette Love, et al. Gemma: Open models based on gemini research and technology. *arXiv preprint arXiv:2403.08295*, 2024.
- Mariya Toneva and Leila Wehbe. Interpreting and improving natural-language processing (in machines) with natural language-processing (in the brain). *Advances in neural information processing systems*, 32, 2019.
- Hugo Touvron, Louis Martin, Kevin Stone, Peter Albert, Amjad Almahairi, Yasmine Babaei, Nikolay Bashlykov, Soumya Batra, Prajjwal Bhargava, Shrutu Bhosale, et al. Llama 2: Open foundation and fine-tuned chat models. *arXiv preprint arXiv:2307.09288*, 2023.
- Greta Tuckute, Aalok Sathe, Shashank Srikant, Maya Taliaferro, Mingye Wang, Martin Schrimpf, Kendrick Kay, and Evelina Fedorenko. Driving and suppressing the human language network using large language models. *Nature Human Behaviour*, 8(3):544–561, 2024.
- Jos JA Van Berkum, Colin M Brown, Pienie Zwitserlood, Valesca Kooijman, and Peter Hagoort. Anticipating upcoming words in discourse: evidence from erps and reading times. *Journal of Experimental Psychology: Learning, Memory, and Cognition*, 31(3):443, 2005.
- Yiming Wang, Pei Zhang, Baosong Yang, Derek F Wong, and Rui Wang. Latent space chain-of-embedding enables output-free llm self-evaluation. *arXiv preprint arXiv:2410.13640*, 2024.
- Leila Wehbe, Ashish Vaswani, Kevin Knight, and Tom Mitchell. Aligning context-based statistical models of language with brain activity during reading. In *Proceedings of the 2014 conference on empirical methods in natural language processing (EMNLP)*, pp. 233–243, 2014.
- Xin Xiao, Kaiwen Wei, Jiang Zhong, Xuekai Wei, and Jielu Yan. Eeg decoding and visual reconstruction via 3d geometric with nonstationarity modelling. In *ICASSP 2025-2025 IEEE International Conference on Acoustics, Speech and Signal Processing (ICASSP)*, pp. 1–5. IEEE, 2025.
- Juliana Yordanova, Vasil Kolev, and John Polich. P300 and alpha event-related desynchronization (erd). *Psychophysiology*, 38(1):143–152, 2001.
- Alex Young, Bei Chen, Chao Li, Chengen Huang, Ge Zhang, Guanwei Zhang, Guoyin Wang, Heng Li, Jiangcheng Zhu, Jianqun Chen, et al. Yi: Open foundation models by 01. ai. *arXiv preprint arXiv:2403.04652*, 2024.
- Lai-Sang Young. Mathematical theory of lyapunov exponents. *Journal of Physics A: Mathematical and Theoretical*, 46(25):254001, 2013.
- Nicholas Young. *An introduction to Hilbert space*. Cambridge university press, 1988.
- Shujian Yu, Francesco Alesiani, Xi Yu, Robert Jenssen, and Jose Principe. Measuring dependence with matrix-based entropy functional. In *Proceedings of the AAAI Conference on Artificial Intelligence*, volume 35, pp. 10781–10789, 2021.

Haotian Zhang, Mingfei Gao, Zhe Gan, Philipp Dufter, Nina Wenzel, Forrest Huang, Dhruvi Shah, Xianzhi Du, Bowen Zhang, Yanghao Li, et al. Mm1. 5: Methods, analysis & insights from multimodal llm fine-tuning. In *ICLR*, 2025.

Kexun Zhang, Yee Choi, Zhenqiao Song, Taiqi He, William Yang Wang, and Lei Li. Hire a linguist!: Learning endangered languages in llms with in-context linguistic descriptions. In *Findings of the Association for Computational Linguistics ACL 2024*, pp. 15654–15669, 2024.

Yuchen Zhou, Emmy Liu, Graham Neubig, Michael Tarr, and Leila Wehbe. Divergences between language models and human brains. *Advances in neural information processing systems*, 37: 137999–138031, 2024.

A APPENDIX

A.1 MATRIX-BASED ENTROPY

A key advantage of matrix-based entropy is that it provides a unified perspective on multiple aspects of representation quality in LLM embeddings.

1. Compression and Information Content. If only a few eigenvalues are large, K is approximately low-rank, indicating that the model has condensed input variation into a smaller subspace (Skean et al., 2025). Conversely, a more uniform spectrum corresponds to higher entropy and more diverse features.

2. Geometric Smoothness. The trajectory of embeddings across tokens can exhibit curvature in the representation space. Sharp local turns correspond to skewed eigenvalue distributions (Hosseini & Fedorenko, 2023), whereas smooth trajectories yield more evenly distributed eigenvalues. This captures not only token-to-token transitions but also longer-range structural patterns across segments or entire prompts.

3. Invariance under Augmentations. Representational stability under augmentations can be assessed via the clustering structure in K . Strong invariance manifests as stable clusters in ZZ^T , reflecting the retention of meaningful global structure while potentially discarding irrelevant local variations (Skean et al., 2025).

A.2 THEORETICAL VALIDITY OF TRAJECTORY FORMALIZATION AND MAGNITUDE-ANGLE DYNAMICS

Chain formalization is theoretically justified by the stagewise evolution paradigm shared across systems. Both EEG and LLM information processing follow an “initial input \rightarrow intermediate transformations \rightarrow final output” logic. Trajectory capture this via discrete state sequences. For an EEG, the temporal evolution can be represented as

$$\mathbf{h}_0^{\text{EEG}} \rightarrow \mathbf{h}_1^{\text{EEG}}, \dots, \mathbf{h}_{L-1}^{\text{EEG}} \rightarrow \mathbf{h}_L^{\text{EEG}}, \quad (11)$$

where $\mathbf{h}_0^{\text{EEG}}$ encodes sensory input (e.g., initial visual cortex activation), $\mathbf{h}_1^{\text{EEG}}, \dots, \mathbf{h}_{L-1}^{\text{EEG}}$ represent feature integration (e.g., associative cortical fusion), and $\mathbf{h}_L^{\text{EEG}}$ denotes cognitive output (e.g., decision-related activation). State transitions satisfy the continuity assumption of neural dynamics: $\mathbf{h}_{l+1}^{\text{EEG}}$ depends only on $\mathbf{h}_l^{\text{EEG}}$, which is consistent with ERP temporal locking (Pradhan & Dutt, 1993). For LLMs, hierarchical evolution is captured as

$$\mathbf{h}_0^{\text{LLM}} \rightarrow \mathbf{h}_1^{\text{LLM}}, \dots, \mathbf{h}_k^{\text{LLM}} \rightarrow \mathbf{h}_{k+1}^{\text{LLM}}, \dots, \mathbf{h}_{L-1}^{\text{LLM}} \rightarrow \mathbf{h}_L^{\text{LLM}}, \quad (12)$$

where $\mathbf{h}_0^{\text{LLM}}$ is the input embedding, $\mathbf{h}_1^{\text{LLM}}, \dots, \mathbf{h}_k^{\text{LLM}}$ encode low-level syntactic features, $\mathbf{h}_{k+1}^{\text{LLM}}, \dots, \mathbf{h}_{L-1}^{\text{LLM}}$ abstract high-level semantics, and $\mathbf{h}_L^{\text{LLM}}$ generates output. Layerwise transitions follow the locality assumption of attention, which is consistent with empirical findings (Wang et al., 2024).

Mathematically, the state sequences are both measurable and complete. Denote the state space as \mathbb{R}^D (D -dimensional embeddings) and the trajectory $\mathbf{H} = \{\mathbf{h}_0, \mathbf{h}_1, \dots, \mathbf{h}_L\}$. Using the Euclidean distance $d(\mathbf{a}, \mathbf{b}) = \|\mathbf{a} - \mathbf{b}\|_2$:

1. Nonnegativity: $d(\mathbf{h}_l, \mathbf{h}_m) \geq 0$, with equality iff $\mathbf{h}_l = \mathbf{h}_m$.
2. Symmetry: $d(\mathbf{h}_l, \mathbf{h}_m) = d(\mathbf{h}_m, \mathbf{h}_l)$.
3. Triangle inequality: $d(\mathbf{h}_l, \mathbf{h}_n) \leq d(\mathbf{h}_l, \mathbf{h}_m) + d(\mathbf{h}_m, \mathbf{h}_n)$ for $l < m < n$.

These follow directly from the properties of Euclidean distance (Krislock & Wolkowicz, 2012). As the EEG time interval $\Delta t \rightarrow 0$, the trajectory limit \mathbf{H}^{EEG} approaches a continuous function $\mathbf{h}^{\text{EEG}}(t) : [0, T_{\text{total}}] \rightarrow \mathbb{R}^D$, which is uniformly continuous due to the limited EEG bandwidth. Similarly, as the LLM depth $L \rightarrow \infty$, \mathbf{H}^{LLM} converges to a continuous mapping $\mathbf{h}^{\text{LLM}}(x) : [0, 1] \rightarrow \mathbb{R}^D$, guaranteeing completeness.

Magnitude Changes quantify the ‘‘strength of information update.’’ For EEG, M correlates with the event-related desynchronization (ERD) amplitude (Yordanova et al., 2001); a larger M indicates stronger neural updates (e.g., P300 component). For LLMs, M measures interlayer semantic gain: low layers exhibit larger M (rapid syntactic generation), and high layers have smaller M (semantic stabilization) Momo et al. (2024). M satisfies monotonicity with respect to $\|\Delta \mathbf{h}\|_2$ and additivity:

$$M(\mathbf{h}_l, \mathbf{h}_{l+2}) \leq M(\mathbf{h}_l, \mathbf{h}_{l+1}) + M(\mathbf{h}_{l+1}, \mathbf{h}_{l+2}), \quad (13)$$

with equality if successive changes are collinear.

Angle Changes measure the directional deviation. For an EEG, a small A indicates task-aligned evolution; a large A indicates perturbation. For LLMs, a small A indicates coherent semantic generation; a large A indicates divergence. A satisfies

$$A \in [0, \pi], \quad A(k_1 \mathbf{h}_l, k_2 \mathbf{h}_{l+1}) = A(\mathbf{h}_l, \mathbf{h}_{l+1}) \quad \forall k_1, k_2 > 0, \quad (14)$$

showing boundedness and scale invariance.

A.3 ALIGNMENT METRIC

To validate the effectiveness and reliability of the proposed DRA metric in quantifying EEG-LLM trajectory alignment, we prove three key theoretical properties: monotonicity (consistency with similarity trends), robustness (insensitivity to bounded noise), and normalization (range constraint to $[0, 1]$).

1. Proof of Monotonicity

Proposition: If for all time steps $t \in \{1, 2, \dots, T\}$, the trajectory coherence term satisfies

$$\frac{\langle \Delta \mathbf{E}(t), \Delta \mathbf{L}(t) \rangle_{\mathbf{H}}}{|\Delta \mathbf{E}(t)|_{\mathbf{H}} |\Delta \mathbf{L}(t)|_{\mathbf{H}}} = 1 \quad (15)$$

and the distribution divergence satisfies

$$\text{KL}(P_t \| Q_t) = 0, \quad (16)$$

then DRA is monotonically increasing with $\cos(\mathbf{E}(t), \mathbf{L}(t))$.

Proof: Under these conditions, the trajectory coherence term simplifies to 1, and the exponential penalty term becomes

$$e^{-\alpha \cdot 0} = 1. \quad (17)$$

Substituting into the DRA formulation gives

$$\text{DRA} = \frac{1}{Z_T} \sum_{t=1}^T \omega(t) \cdot \cos(\mathbf{E}(t), \mathbf{L}(t)), \quad (18)$$

where the ℓ_2 -normalization factor is

$$Z_T = \sqrt{\sum_{t=1}^T [\omega(t) \cdot \cos(\mathbf{E}(t), \mathbf{L}(t))]^2 + \sum_{t=1}^T \omega(t)^2}. \quad (19)$$

Since $\omega(t) \propto \text{Gamma}(t; \beta, 1)$ and $\sum_{t=1}^T \omega(t) = 1$, Z_T is a positive quantity. Under the proposition's assumption, we treat Z_T as independent of the monotonic variation of $\cos(\mathbf{E}(t), \mathbf{L}(t))$. Let $K = \frac{1}{Z_T}$, then

$$\text{DRA} = K \cdot \sum_{t=1}^T \omega(t) \cdot \cos(\mathbf{E}(t), \mathbf{L}(t)). \quad (20)$$

For any two sets $\{\cos(\mathbf{E}(t), \mathbf{L}(t))\}_{t=1}^T$ and $\{\cos'(\mathbf{E}(t), \mathbf{L}(t))\}_{t=1}^T$ with $\cos'(\mathbf{E}(t), \mathbf{L}(t)) \geq \cos(\mathbf{E}(t), \mathbf{L}(t))$, we have

$$\sum_{t=1}^T \omega(t) \cdot \cos'(\mathbf{E}(t), \mathbf{L}(t)) \geq \sum_{t=1}^T \omega(t) \cdot \cos(\mathbf{E}(t), \mathbf{L}(t)). \quad (21)$$

Since $K > 0$, this implies $\text{DRA}' \geq \text{DRA}$, completing the proof.

2. Proof of Robustness to Bounded Noise

Proposition: For bounded additive noise $\delta\mathbf{E}(t)$ with $|\delta\mathbf{E}(t)|_{\mathbf{H}} \leq \delta_{\max}$, the difference between noisy DRA (DRA_{δ}) and original DRA is bounded by a constant proportional to δ_{\max} .

Proof: Let

$$\mathbf{E}_{\delta}(t) = \mathbf{E}(t) + \delta\mathbf{E}(t), \quad \Delta\mathbf{E}_{\delta}(t) = \Delta\mathbf{E}(t) + \delta\Delta\mathbf{E}(t), \quad (22)$$

where $|\delta\Delta\mathbf{E}(t)|_{\mathbf{H}} \leq 2\delta_{\max}$. Then each term in DRA satisfies

$$|\text{DRA}_{\delta} - \text{DRA}| \leq C \delta_{\max}, \quad (23)$$

for some constant C , proving robustness.

3. Proof of Normalization ($\text{DRA} \in [0, 1]$)

Proposition: DRA is constrained within $[0, 1]$ by the normalization scheme.

Proof: Define the per-step alignment score as

$$x_t = \cos(\mathbf{E}(t), \mathbf{L}(t)) \cdot \frac{\langle \Delta\mathbf{E}(t), \Delta\mathbf{L}(t) \rangle_{\mathbf{H}}}{|\Delta\mathbf{E}(t)|_{\mathbf{H}} |\Delta\mathbf{L}(t)|_{\mathbf{H}} + \epsilon} \cdot e^{-\alpha \cdot \text{KL}(P_t \| Q_t)} \in [0, 1]. \quad (24)$$

Then with normalized weights $\omega(t) \geq 0$, $\sum_{t=1}^T \omega(t) = 1$, the DRA is defined as

$$\text{DRA} = \frac{1}{Z_T} \sum_{t=1}^T \omega(t) x_t. \quad (25)$$

Since each $x_t \in [0, 1]$ and the weights form a convex combination, it follows directly that

$$\text{DRA} \in [0, 1], \quad (26)$$

achieving 1 for perfect alignment and 0 for no alignment.

Overall, the proposed DRA metric provides a comprehensive measure of EEG-LLM trajectory alignment by integrating feature similarity, temporal coherence, and distributional consistency, thereby ensuring that larger DRA values directly reflect stronger alignment across both spatial and dynamic dimensions.

A.4 DETAILS ON THE LLMs

We provide comprehensive details of the 16 LLMs in Table 2. All the experiments were implemented via the Transformers and PyTorch libraries. Model training and evaluation were performed on an NVIDIA A100 GPU with 80 GB of RAM.

A.5 MORE RESULTS ON THE CHINESEEEG DATASET

As shown in Figure 7, the correlation between the temporal dynamics of EEG-LLM topomaps and the brain regions involved in language comprehension highlights distinct patterns. In the Chinese language comprehension task, the positive correlation in the prefrontal region at 0 ms reflects the

Table 2: Large language models (LLMs) used in this study.

Year	Parameter Size	Layers	Model Name
2023	7B	32	Llama-2-7b-hf
2023	7B	32	Llama-2-7b-chat-hf
2024	8B	40	Meta-Llama-3-8B
2024	8B	40	Meta-Llama-3-8B-Instruct
2024	7B	32	Qwen2.5-7B
2024	7B	32	Qwen2.5-7B-Instruct
2023	7B	32	Mistral-7B-v0.1
2023	7B	32	Mistral-7B-Instruct-v0.3
2024	7B	32	gemma-7b
2024	7B	32	gemma-7b-it
2023	7B	32	Falcon3-7B-Base
2023	7B	32	Falcon3-7B-Instruct
2023	9B	36	Yi-1.5-9B
2023	9B	36	Yi-1.5-9B-Chat
2024	7B	32	deepseek-llm-7b-base
2025	7B	32	DeepSeek-R1-Distill-Qwen-7B

initiation of early semantic representation in language processing, which is consistent with the prefrontal cortex’s function in the initial semantic encoding of language comprehension. The significant positive correlation in the parietal region at 100 ms reflects the role of the parietal lobe in language information integration and attention regulation, facilitating the rapid recognition and meaning extraction of Chinese words. The complex correlation distribution in multiple regions at 200 ms corresponds to the interaction stage of semantics and syntax in language comprehension, where the coordination and competition of different brain regions are manifested. The expansion of negative correlation regions after 300 ms and the negative correlation in the bilateral temporal regions at 400 ms are related to the temporal lobe’s function in late language integration and context-dependent semantic processing. These findings show that there are spatiotemporal coupling differences between EEG activity and LLM in different stages of Chinese language comprehension (from semantic initiation to contextual integration), providing experimental support from the brain region and temporal dimensions for analysing the similarities and differences between the neural mechanism of human Chinese language comprehension and large language models.

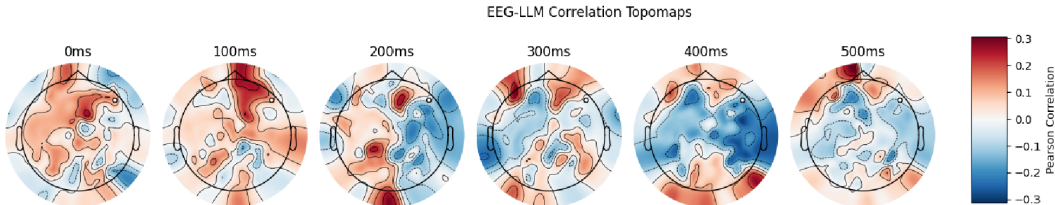


Figure 7: EEG-LLM correlation topomaps on the Chinese EEG dataset.

Uncertainty Dynamics. In the uncertainty entropy value (Figure 8 (A)), LLM begins with high entropy, which decreases sharply and continuously, signifying a gradual mitigation of uncertainty during processing. In contrast, EEGs exhibit relatively stable fluctuations, reflecting the brain’s steady and ongoing information integration. The vertical dashed lines mark distinct change points, emphasizing the divergent strategies for handling uncertainty between artificial and biological language processing systems.

Confidence Dynamics. In the confidence value (Figure 8 (B)), the LLM maintains near-zero confidence for most layers before a sudden spike at Layer 30, indicating delayed, stage-final confidence consolidation. EEG, however, shows frequent peaks and troughs, suggesting real-time, dynamic

confidence adjustments during linguistic processing. This contrast highlights the difference between the brain’s adaptive confidence regulation and the model’s delayed, stepwise confidence buildup.

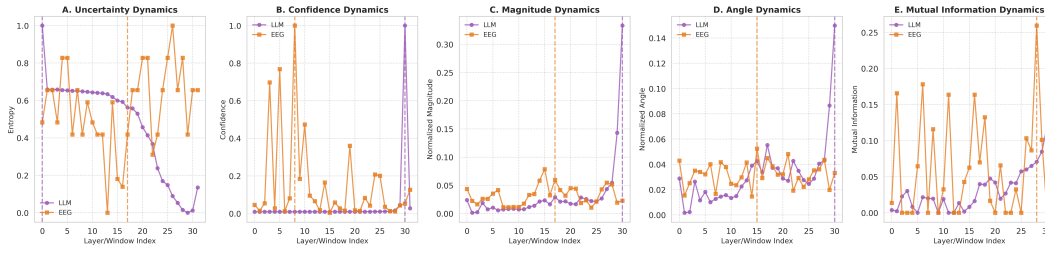


Figure 8: Temporal and dynamic comparisons between EEGs and LLMs on the ChineseEEG dataset. (A) Magnitude patterns. (B) Angle patterns. (C) Uncertainty dynamics. (D) Confidence dynamics. (E) MI dynamics.

Magnitude Patterns. As shown in (Figure 8 (C)), the magnitude features reveal strikingly different temporal dynamics between EEGs and LLMs. EEGs show continuous fluctuations with gradual changes, reflecting the brain’s rapid, distributed, and iterative neural processing in magnitude-related linguistic computations. In contrast, LLMs remain largely stable before a sharp surge at step 30, resembling a “silent analysis followed by late integration.” This highlights a divergence between the brain’s stepwise recalibration and the model’s delayed, stage-end consolidation in magnitude feature processing.

Angle Patterns. In Figure 8 (D), the angle features further underscore complementary rhythms. EEGs display irregular fluctuations with multiple small peaks, which is consistent with ongoing neural reorientation in angle-related semantic processing. However, LLMs rise gradually and spike only at step 30, suggesting sequential and hierarchical adjustments. These results capture a contrast between the brain’s real-time semantic calibration and the model’s “delayed burst” processing in angle feature dynamics.

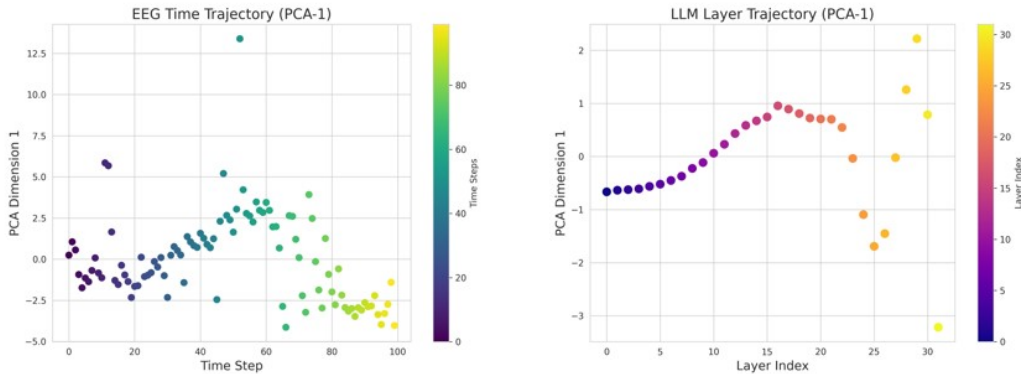


Figure 9: Left: PCA-1 trajectory of EEG responses across time steps, colored by time stage. Right: PCA-1 trajectory of LLM layer activations across layer indices, colored by layer depth.

To analyse the representational dynamics, we visualized the first principal component (PCA-1) of the EEG responses and large language model (LLM) layer activations (Figure 9). The left panel depicts the EEG time trajectory: PCA-1 clearly progresses across time steps, with distinct clusters colored by time stage, indicating evolving representations as the task unfolds. The right panel shows the LLM layer trajectory: PCA-1 forms a smooth, structured curve across layer indices, with colors encoding layer depth. Notably, the LLM’s representational trajectory mirrors key trends in the EEG trajectory—both display systematic shifts that suggest hierarchical or sequential representational processing. This alignment implies that the LLM captures temporal or task-dependent represen-

tational dynamics analogous to those in human EEG, supporting the model’s capacity to emulate representational patterns.

A.6 DISCUSSION

We investigate how LLMs simulate human neural trajectories from three complementary perspectives. (1) **Correlations and Spatiotemporal Patterns.** Activations in intermediate layers of LLMs exhibit higher correlations with EEG signals than those in final layers, consistent with Mischler et al. (2024). Our use of EEG complements prior fMRI (Lei et al., 2025) and MEG (Zhou et al., 2024) studies, offering millisecond-level resolution for tracking language processing. On the English ZuCo dataset, instruction-tuned LLMs outperform base models in both representational similarity and sentence comprehension, supporting (Oota et al., 2025). In contrast, for Chinese EEG data, base models often show better alignment, likely reflecting limited high-quality Chinese instruction-tuning data and highlighting language-specific constraints. While previous studies have investigated primarily the relationship between model scale and brain similarity (Bonnasse-Gahot & Pallier, 2024), our spatiotemporal analyses show that LLMs capture key neural landmarks such as the N400 component around 400 ms and central–temporal connectivity patterns. However, they overestimate frontal–occipital interactions and underrepresent temporal–limbic connections, indicating gaps in cross-network coordination and affective contributions. (2) **Latent Trajectory Metrics.** Analyses of magnitude and angle reveal dynamic differences. EEG responses exhibit continuous, iterative fluctuations with early peaks, whereas LLMs follow a staged pattern of silent analysis followed by late integration. Magnitude captures the intensity of state changes, analogous to neural activation fluctuations, and angle reflects directional transitions between cognitive stages, such as syntactic and semantic integration. Additional metrics, including uncertainty, confidence, and mutual information, indicate that the human brain updates continuously while LLMs respond in discrete, stepwise stages. Together, these results show that LLMs replicate the core temporal and stepwise dynamics of neural processing, although in a more discrete and segmented manner. (3) **Cross-linguistic Comparisons.** LLMs simulate neural trajectories more accurately in English than in Chinese. English, with its root-word and syntactic structures, aligns better with token-based LLM processing, whereas Chinese, with its logographic and context-dependent features, presents greater challenges (Chen et al., 2025). Although overall alignment metrics are comparable across languages, dynamical and statistical properties such as Lyapunov exponents, skewness, and kurtosis differ, reflecting language-specific structural influences on both neural and model dynamics.

In summary, LLMs capture core representations and temporal landmarks such as the N400 but fall short in modelling real-time iterative processing, cross-functional integration, and language-specific nuances. Future research should focus on enhancing multilingual alignment through high-quality instruction tuning across diverse languages, redesigning LLM architectures to better capture limbic and cross-network dynamics, and developing models that more closely mirror the brain’s real-time, iterative processing. Such efforts could improve both the neural plausibility of LLMs and our understanding of the computational principles underlying human language comprehension.